Energy Transfer for Leaky Surface Plasmon Polaritons in Gold Nanostripes

Janak Bhandari and Gregory V. Hartland*

Department of Chemistry and Biochemistry
University of Notre Dame
Notre Dame, IN 46556
United States

Abstract: The properties of the leaky surface plasmon polariton (SPP) modes in gold nanostripes were investigated using scattered light microscopy. Both bare gold nanostripes and stripes coated with a thin polymer film containing a near-infrared absorbing dye were examined. Real-space microscopy images were employed to determine the SPP propagation length, while Fourier space images provided measurements of the wavevector. Frequency versus wavevector dispersion curves were generated by performing experiments at different excitation wavelengths, and the slopes of these curves yielded the SPP group velocities. For the bare nanostripes the group velocity was determined to be $v_g = (0.92 \pm 0.05)c_0$ and for the dye-coated nanostripes it was $v_g = (0.85 \pm 0.06)c_0$, where c_0 is the speed of light. The SPP lifetimes were estimated by combining the group velocity and propagation length measurements. The results show that the lifetime of the gold SPPs is significantly reduced when the nanostripes are coated with the dye. At the peak of the dye absorption curve the change in the SPP dephasing rate induced by the dye-polymer film was found to be $0.07\ \mathrm{fs}^{-1}$. Finite element simulations show that the increased dephasing is due to a combination of energy transfer from the SPP modes to the dye, as well as increased radiation damping due to changes in the dielectric environment of the nanostructures. These findings provide insights into the energy transfer processes in plasmonic systems, which can be leveraged to optimize the design of plasmonic devices for applications in sensing, imaging and nanophotonic circuits.

* Corresponding Author; e-mail: ghartlan@nd.edu

1. Introduction:

Propagating Surface Plasmon Polaritons (SPPs) are guided electromagnetic waves that move along the interface between a metal and a dielectric.[1-2] The unique properties of SPPs, such as their ability to confine light below the diffraction limit,[3] enhance electromagnetic fields[4] and move over long distances,[5] have made them a subject of extensive research in nano-photonics and plasmonics.[6-7] This includes the development of advanced optoelectronic devices, such as sensors,[8] solar cells,[9] and light-emitting devices.[10-11] When semiconductor or molecular systems are in close contact with plasmonic nanostructures plasmon-exciton coupling can occur, for both propagating SPPs and localized surface plasmon resonances (LSPRs) of particles.[12-16] Plasmon-exciton interactions can be categorized into weak and strong coupling regimes, and the coupling strength is characterized by the Rabi frequency for energy exchange between the plasmons and excitons.[12, 16-17]

In the strong coupling regime, where the Rabi frequency is larger than the dephasing rates of the system, the interaction leads to the formation of hybrid states known as plexitons,[13] that are separated in the frequency domain. Conversely, in the weak coupling regime the two hybrid states are not resolved, and the electromagnetic modes and wave functions of plasmons and excitons are, to first order, the same as the non-interacting states.[15] However, energy transfer still occurs between the plasmons and excitons, which can substantially impact the properties of the system, such as modifying the plasmon lifetime.[18, 19] Field enhancements and Purcell effects also occur even for the weakly coupled systems, which affect the absorption cross-sections and radiative rates, respectively, of the semiconductor or molecular systems coupled to the plasmons.[20-22] The major factor that determines whether a system is in the strong or weak coupling regime is the strength of the optical transitions of the semiconductor/molecular system.[23]

The majority of the plasmon-exciton coupling experiments reported to date have been for LSPRs.[13-19] For example, the way adsorbed molecular and semiconductor species affect the LSPR linewidth of nanoparticles has been examined by several groups.[18-19, 24-26] The motivation for many of these studies is to understand plasmon enhanced catalysis, which typically involves electron transfer events rather than energy transfer.[27] In cases where energy transfer has been

identified as the broadening mechanism,[25] changes in linewidth as high as ~100 meV have been identified, with efficiencies up to 50%.[18-19] This indicates that energy transfer can be very fast, even when there is only weak coupling between the optical transitions of the dye and the particle LSPR. Energy transfer between propagating SPPs and adsorbed dye molecules has been less studied. Previous work includes imaging experiments to measure the SPP propagation lengths.[28-30] However, these measurements did not report rates/timescales for energy transfer.

In this paper coupling between propagating SPPs in lithographically fabricated gold nanostripes and the optical transitions of a near-IR dye is investigated. Lithographically fabricated rather than chemically synthesized metal nanostructures were used for several reasons, including control over dimensions and high reproducibility between structures.[31-33] This allows us to average data over different structures and, thus, increase the accuracy of the measurements. Interrogating structures with well-defined dimensions also allows meaningful comparisons to finite element simulations.[31-33] However, a disadvantage is that the dielectric constants of Au nanostructures created by nanolithography are generally inferior (more lossy) that the single crystal structures that can be made by wet chemical methods.[34] Strong plasmon-exciton coupling is not observed for our system. However, significant changes in the propagation length of the SPPs occurs upon coating the nanostripes with the dye. By comparing dye coated and uncoated nanostructures we are able to determine the timescale for SPP dephasing induced by the dye film.[33] The increase in SPP dephasing from the dye film follows the absorption spectrum of the dye, indicating energy transfer between plasmons and excitons.[18-19] However, finite element simulations show that both energy transfer to the dye and increased radiation losses due to changes in the dielectric environment of the nanostripes affect SPP dephasing. This is a somewhat unexpected result, that is important for understanding how plasmonic structures can be engineered to enhance light-matter interactions in practical applications.

2. Methods:

Fabrication of Gold Nanostripes: Gold nanostripes on #1.5 borosilicate glass substrates were fabricated using standard electron-beam lithography, metal deposition, and liftoff

procedures. The stripes were designed to be 3 μm wide and 100 μm long. In the fabrication process a 3 nm titanium adhesion layer was first deposited, followed by a 50 nm gold layer using electron-beam evaporation. To examine plasmon-molecule interactions, a near-IR Croconaine dye in a polyvinyl alcohol (PVA) solution was spin-coated onto the substrates.[35] The thickness of the PVA layer was estimated to be approximately 25 nm with a refractive index of 1.5 by ellipsometry measurements (Gaertner L117 Ellipsometer). Experiments were conducted on both uncoated nanostripes, nanostripes coated with the dye-PVA thin film, and nanostripes coated with a PVA thin film without dye. Examining the different structures allows quantitative information to be obtained about energy transfer to the dye.

Optical Measurements: The samples were placed on an inverted optical microscope (Olympus IX-71). A diagram of the experimental setup is presented in Figure S1 of the Supporting Information. The nanostripes were optically excited with the output of a Ti:Sapphire oscillator (Coherent, Chameleon Ultra II) that operated in the 700-1000 nm wavelength range. The laser beam was tightly focused through the glass substrate using a high numerical aperture (NA) oil-immersion objective lens (Olympus UPlanFL N, 100x, NA = 1.3). SPPs were launched by positioning the end of the nanostripe in the laser focus with a motorized stage (Mad City Labs MCL-uS).[36-37] The laser polarization was adjusted to be parallel to the long axis of the structures. Scattered light from the sample was collected with the focusing objective and directed to a CMOS camera (Basler Powerpack Microscopy Camera, Pulse 5.0 MP). Specifically, a 4-f optical configuration was used to image the back focal plane of the objective onto the camera, thus, mapping the in-plane wave-vector distribution of the scattered light into a conjugate Fourier plane.[38-40] Real-space images were captured by placing a lens in front of the camera at its focal distance.[31, 33, 38-40] An aperture in the conjugate object plane of the microscope was used to block directly scattered light from the excitation beam. The Fourier space and real space images were used to measure the SPP wavevector (k_{SPP}) and propagation length (L_{SPP}), respectively. Measurements were taken from at least three different nanostripes to determine average values and confidence limits for k_{SPP} and L_{SPP}. The absorption spectrum of the near-IR croconaine dye-PVA film was recorded with a Jasco UV-670 UV-vis spectrophotometer.

Finite Element Simulations: Finite element simulations of the nanostripe SPP modes were performed in COMSOL Multiphysics (v. 5.3) using a two-dimensional mode analysis calculation.[40-42] In this two-dimensional model the nanostripes are reduced to rectangles with a height of 50 nm and width of 3 μm. Note that the two-dimensional simulations effectively assume infinitely long nanostripes. This is appropriate when the length of the nanostripe is much longer than the SPP propagation length, which is the case for our system. A 3 nm Ti adhesion layer was included between the nanostripes and the glass substrate in the simulation to match the experimental system. Values for the refractive indices of Au and Ti were taken from COMSOL's library of materials, which uses the refractive index data for Au from Ref. [43]. The refractive index of the glass was set to $n = 1.45$ (the value from COMSOL for silica glass). The finite element simulations yield the complex effective mode index for the system $n_{eff} - i\,\alpha/k_0$, where the real part gives the SPP wavevector $k_{SPP} = n_{eff}k_0$, and the imaginary part is related to the propagation length by $L_{SPP} = 1/2\alpha$.[31, 33, 38, 40-42] More details about the simulations, including additional plots of SPP dispersion curves and L_{SPP} versus wavelength, are presented in the Supporting Information. Note that more recent Au refractive index data is available than that in Ref. [43]. Comparison between the different data sets shows that sample preparation has a significant effect on the dielectric constants.[34] Thus, for our nanofabricated samples it is not clear which data set is the best to use.[34, 43] However, the main point of the simulations in this paper is to investigate the effect of dye coating on the SPP lifetime. This analysis involves subtracting results for bare and coated structures, so that the exact choice of dielectric constant data is not expected to be a significant.

3. Results and Discussion:

Before discussing the experimental data, it is useful to visualize the SPP modes in the system. Figure 1 shows plots of the norm of the electric field for the different SPP modes of a nanostripe. In this figure the horizontal line represents the interface, with glass on the bottom and air on top, and rectangle is the nanostripe. Two types of modes occur: leaky modes where the field is at the metal-air interface (Figs. 1(a) and (b)), and bound modes where the field is localized at the metal-glass interface (Figs. 1(c) and (d)).[31, 33] The wavevectors of the bound

modes are too large for these modes to be observed in regular far-field optical microscopy experiments – the value of n_{eff} for the mode must be less than the NA of the objective for scattered light to be collected by the microscope. However, the wavevectors for the leaky modes are only slightly larger than the light line, and these modes can be imaged by using a high NA oil immersion objective.

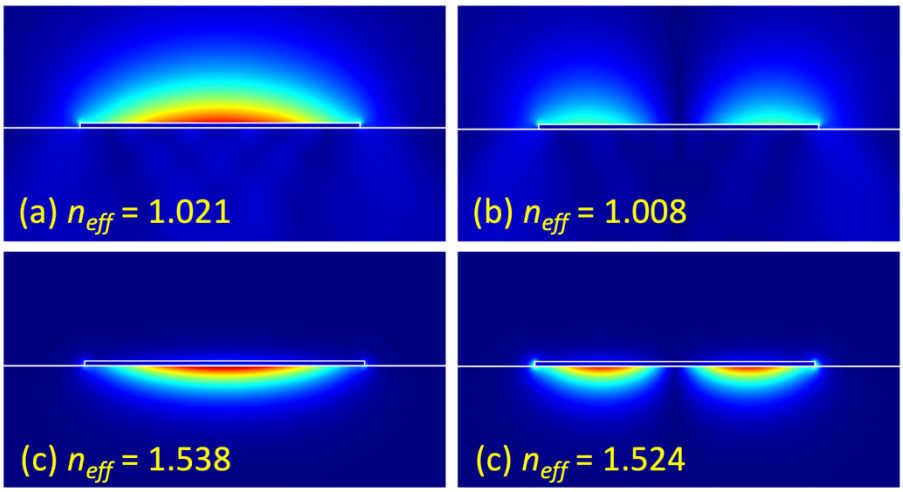

Figure 1: Mode plots of the first- and second-order leaky SPP modes (panels (a) and (b)), and the first- and second-order bound SPP modes (panels (c) and (d)). The wavelength was 0.75 μm and the effective indices of the modes are given in the figure. Higher order modes exist, but they are not typically observed in experiments. The horizontal line in these images represents the interface between glass (bottom) and air (top). A thin Ti wetting layer is included in the simulations, but it can't be discerned in these plots.

Figure 2(a) shows a transmitted light image of a lithographically fabricated Au nanostripe used in the experiments. The nanostripes have a uniform width and are slightly rounded at the ends. Figure 2(b) shows the real-space image of propagating SPPs in the nanostripe obtained by focusing 0.73 μm light at the end of the structure. Scattered light from the leaky SPP mode is observed at the edges of the nanostripe, with the intensity gradually decreasing down the length of the nanostripe due to resistive heating (creation of excited electrons through SPP dephasing) and radiation losses.[31] Figure 2(c) shows a line profile of the scattered light along one of the edges. Fitting to an exponential decay gives a propagation length of 9.7 μm for this nanostripe.

The structure in the real space-image arises from interference between the reflected light from the laser beam and the scattered light from the leaky SPP mode.[31] The propagation lengths reported below were the average of at least three nanostripes, and the errors were determined from the standard deviations.

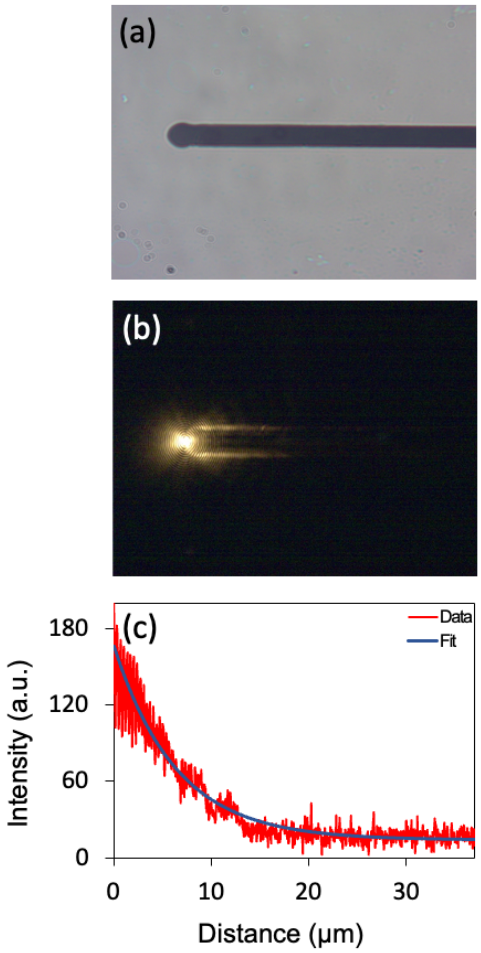

Figure 2: (a) Transmitted light image of a Au nanostripe. (b) Real-space image of the leaky SPP mode in a 3 μm wide Au nanostripe obtained with 0.73 μm excitation. (c) Line profile of the scattered light taken from one of the edges of the stripe in the real-space image, along with an exponential fit (an offset has been added to account for the background scattered light).

Figure 3(a) shows an example Fourier space image of the leaky SPP mode for a Au nanostripe. For these experiments an aperture was placed in the conjugate image plane (see Figure S1) and positioned so that the directly reflected laser beam was blocked, and scattered light was only collected from the lower portion of the nanostripe. The vertical line in the images

indicates the SPP wavevector. A diagram that shows the momentum matching conditions for the leaky SPP mode and photons in the glass substrate is presented in Figure S2 of the Supporting Information. The SPP wavevectors were measured as a function of frequency for at least three separate nanostripes, and the results were averaged together. Figure 3(b) shows the dispersion curves for bare Au nanostripes (red markers), Au nanostripes coated with PVA (light blue markers) and dye-PVA coated nanostripes (dark blue markers). The dashed lines are fits to the experimental data, and the orange line is the light line for free space photons ($\omega = c_0 k_0$). The group velocities were determined from the slope of the dispersion curves by $v_g = \partial\omega/\partial k$.[1-2] The values obtained are $v_g = (0.92 \pm 0.05)c_0$ for the bare nanostripes, $v_g = (0.87 \pm 0.05)c_0$ for the PVA coated nanostripes, and $v_g = (0.85 \pm 0.06)c_0$ for the dye-PVA coated nanostripes. Note that the measured dispersion curve for the bare nanostripes is almost exactly the same as the curves calculated through finite element simulations. This indicates that the dielectric constant data from Ref. [43] is a reasonable choice for these samples.

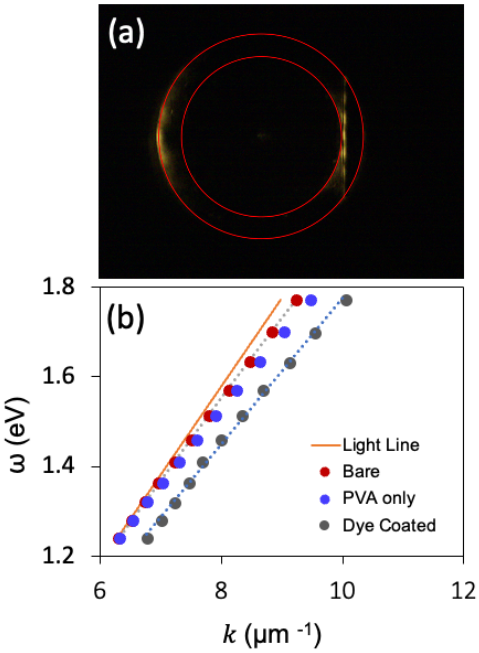

Figure 3: (a) Fourier-space image of SPPs for a Au nanostripe. The image was recorded with an excitation wavelength of 0.73 μm. The inner circle shows the condition for total internal reflection ($k = k_0$) and the outer circle shows the maximum wavevector that can be recorded with our imaging system ($k = NA$). (b) ω versus k dispersion curves for bare nanostripes and nanostripes

coated with PVA and dye-PVA thin films. The orange line is the light line $\omega = c_0 k_0$, and the dashed lines show fits to the data. Error bars are contained within the symbols.

The propagation lengths measured for the bare and dye-PVA coated nanostripes are presented in the Supporting Information. Figure 4(a) shows the lifetimes of the SPP modes for the bare and dye-PVA coated nanostripes obtained by dividing the propagation lengths by the group velocity: $\tau = L_{SPP}/v_g$.[44] It is important to note that the SPP lifetimes for the bare and coated nanostripes are similar at high and low wavelengths, however, at intermediate wavelengths coating the nanostripes with a thin film containing dye significantly decreases the SPP lifetime. The rate constants for SPP decay induced by the dye were determined by $k_{dye} = 1/\tau_{dye} - 1/\tau_{Au}$, where τ_{dye} and τ_{Au} are the lifetimes for the nanostripes coated with the dye-PVA film and the bare nanostripes, respectively. Note that coating the nanostripes with a PVA film without dye has a small effect on the SPP lifetime (see Figure S4 of the Supporting Information). Thus, using the PVA coated nanostripes as the reference in the k_{dye} calculation rather than the bare nanostripes does not significantly change the values of k_{dye} (see Figure S5 of the Supporting Information). Figure 4(b) shows a plot of k_{dye} versus wavelength. The rate constant curve follows the absorption spectrum of the dye-PVA film, which is presented in Figure 4(c). This implies that energy transfer from the leaky SPP mode to the dye is a possible explanation for the increase in SPP damping. However, to fully understand the mechanism for the decrease in the SPP lifetimes induced by the dye-PVA films, we need to consider the different processes that can cause SPP damping for coated nanostructures.

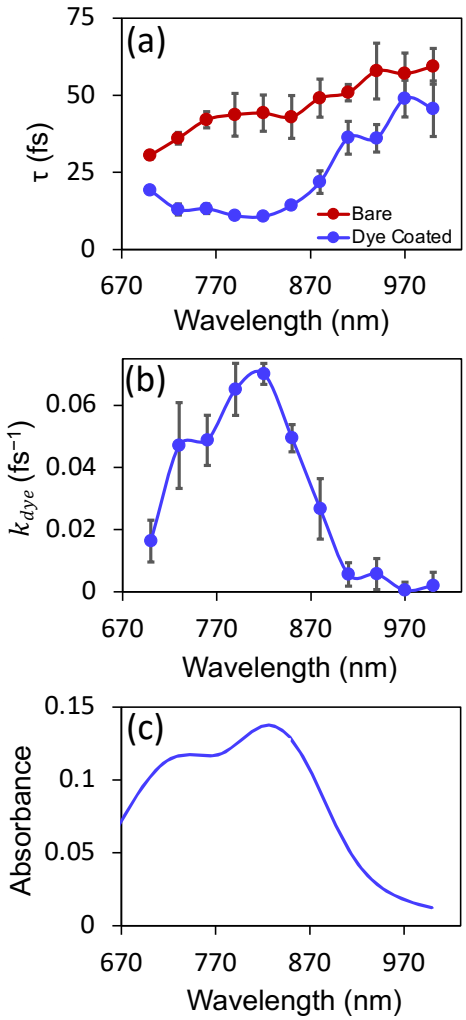

Figure 4: (a) Lifetimes of the leaky SPP mode for bare (red) and dye-PVA coated nanostripes (blue) as a function of excitation wavelength. (b) Rate constants (k_{dye}) for energy loss from the SPP modes induced by the dye-PVA film. (c) Absorption spectrum of the dye-PVA film. Note that the spectrum of the dye in the film is slightly red shifted compared to the spectrum of the dye in solution.[35]

There are several possible reasons for the decrease in the lifetimes/propagation lengths when the nanostripes are coated with a thin film that are not energy transfer. First, surface roughness of the film could give rise to scattering effects, which would reduce the SPP propagation length. Adding molecules to the surfaces of the nanostripes can also cause chemical interface damping (CID).[24-26] Previous work has shown that CID causes changes in the SPP

propagation lengths of Au nanostripes with similar dimensions to those in this study, although the effects are not large.[33] However, CID and surface roughness should be present in both the PVA and dye-PVA films. The observation that the lifetimes/propagation lengths are similar for the nanowires coated with PVA only and the bare nanostripes, shows that CID and surface roughness are minor effects. In addition, neither surface roughness nor CID are expected to be wavelength dependent. For these reasons we do not believe that surface roughness and/or CID are responsible for the wavelength dependent changes in k_{dye} reported in Figure 4(b).

Coating with a thin film also changes the refractive index environment around the nanostripes, which can change the SPP field. Finite element simulations of nanostripes coated with a thin non-absorbing film with different refractive index values show significant changes in the propagation lengths, which arise from changes in both radiative damping and resistive heating in the gold (see Supporting Information for details). Thus, to determine whether k_{dye} is controlled by energy transfer to the dye, or changes in the field distribution of the leaky SPP mode due to changes in the refractive index environment of the nanostripes, a Lorentz oscillator model was used to simulate the absorption/dispersion properties of the dye-PVA film.[45] In this model the dielectric constant of the film is written as

$$\epsilon = \epsilon_b + \sum_{i=1,2} \frac{f_i \omega_i^2}{\omega_i^2 - \omega^2 - i\omega\gamma_i} \qquad (1)$$

where ϵ_b is the background dielectric constant of the film, and f_i, ω_i and γ_i are the oscillator strength, resonant frequency and damping of the optical transitions of the dye, respectively. In our analysis ϵ_b was set to 2.25 (to match PVA),[45] and ω_1 f_1, γ_1, ω_2, f_2 and γ_2 were adjusted to match the form of the absorbance spectrum of the sample (Figure 4(c)), and give a propagation length for the dye-coated nanostripes that roughly matches the experimental values (Figure 4(b)). The values of the parameters used in Equation (1), and the corresponding complex refractive index data are given in the Supporting Information. Note that the parameters for the Lorentz oscillator function are not physically meaningful, they are simply adjusted to match the spectrum of the dye-PVA film.

Figure 5(a) and (b) show the dispersion curves and propagation lengths for bare gold nanostripes and the dye-PVA coated nanostripes obtained from the COMSOL mode analysis

simulations. In these simulations energy transfer to the dye appears as resistive heating in the polymer layer. Coating with a dye-PVA film causes a significant change in the dispersion curve, consistent with the experimental measurements in Figure 3(b). Both the dispersion curves and the propagation lengths are in reasonable agreement with the experimental measurements (see Figure S4(a) of the Supporting Information). The propagation lengths were converted to lifetimes using the group velocities, which were determined from Figure 5(a). For the bare nanostripes we find a group velocity of $0.902c_0$ for the simulations. For the dye coated nanostripes the dispersion curve is not a straight line, which means that the group velocity changes with k_{SPP}. We find a group velocity of $(1.3041 - 0.0552k_{SPP})c_0$ for the dye coated nanostripes. The rate constants for SPP decay induced by the dye-PVA layer were then calculated by $k_{dye} = 1/\tau_{dye} - 1/\tau_{Au}$. The results are presented in Figure 5(c). The form of the k_{dye} versus wavelength plot is consistent with the experiments, and follows the calculated absorption spectrum of the dye (see Figure 4). The good match in the absolute value of k_{dye} for the simulations and experiments is because the oscillator strength of the dye-PVA layer was adjusted to match the experimental propagation lengths. Note that the simulations do not correctly reproduce the experimental dispersion curve for the PVA only coated nanostripes. However, this is most likely a problem with the experiments (the PVA film is not the same as that prepared with the dye, for example, it may have a different thickness) rather than the simulations. Overall, these results show that the finite element analysis correctly captures the behavior of the dye-coated nanostripes. We now look at the different contributions to the k_{dye} versus wavelength curve.

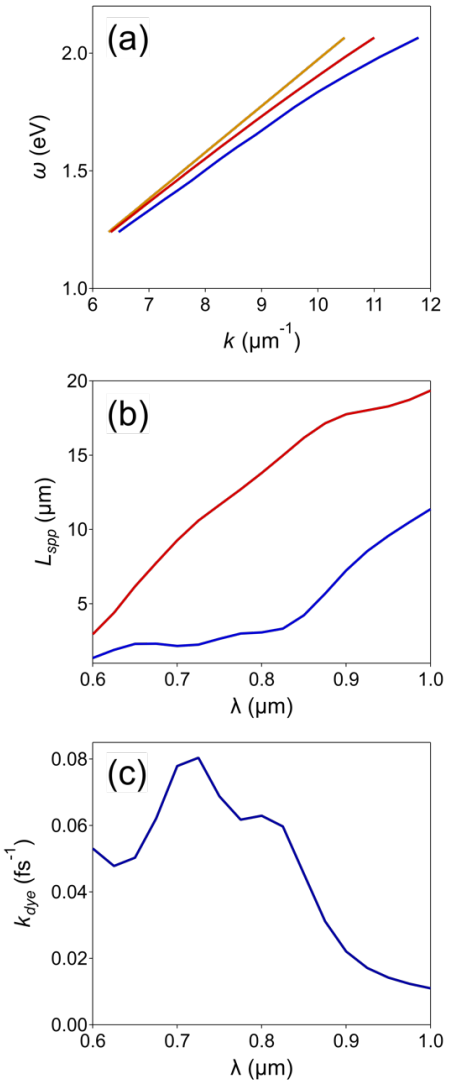

Figure 5: (a) Calculated dispersion curves for bare Au nanostripes (red) and Au nanostripes coated with a 25 nm thick dye-PVA film (blue). The orange line is the light line. (b) Calculated propagation lengths for bare and dye-PVA coated nanostripes, same color scheme as panel (a). (c) k_{dye} versus wavelength determined from the calculated propagation lengths and group velocities.

The relative contributions to SPP dephasing from radiation damping (η_{rad}) and resistive heating effects in the metal (η_{Au}) and dye-polymer layer ($\eta_{polymer}$) can be determined from the relative power losses for the different processes. Note that in our model resistive heating in the polymer corresponds to energy transfer from the SPP mode to the dye. For the two-dimension finite element simulations used here, the power dissipated by radiation is calculated by

integrating the time-average Poynting vector $\langle\vec{S}\rangle$ over a line that encloses the nanostripe (see Supporting Information), and the contributions from resistive heating in the gold and polymer are calculated by integrating the resistive losses (Q_{rh} in COMSOL language) over the metal and polymer domains. Specifically,

$$\eta_{rad} = \frac{\oint \vec{n}.\langle\vec{S}\rangle dl}{\oint \vec{n}.\langle\vec{S}\rangle dl + \iint_{metal} Q_{rh} dA + \iint_{poly} Q_{rh} dA} \quad (2a)$$

$$\eta_{Au} = \frac{\iint_{metal} Q_{rh} dA}{\oint \vec{n}.\langle\vec{S}\rangle dl + \iint_{metal} Q_{rh} dA + \iint_{poly} Q_{rh} dA} \quad (2b)$$

$$\eta_{polymer} = 1 - \eta_{rad} - \eta_{Au} \quad (2c)$$

where $\vec{n}$ is the outward normal unit vector, and the metal domain includes contributions from the Ti wetting layer. The different contributions to the SPP attenuation coefficient are then simply given by $\alpha_i = \eta_i \alpha_{tot}$ where α_{tot} is the total attenuation from the complex effective mode index for the system ($n_{eff} - i\,\alpha/k_0$). The values of α_i for radiation losses and resistive heating for the bare and dye-PVA coated nanowires are plotted versus wavelength in Figure S9. The experimental results in Figure 4(b) represent the difference in attenuation for the dye coated and bare nanostripes. This is plotted in Figure 6(a) for the simulation results.

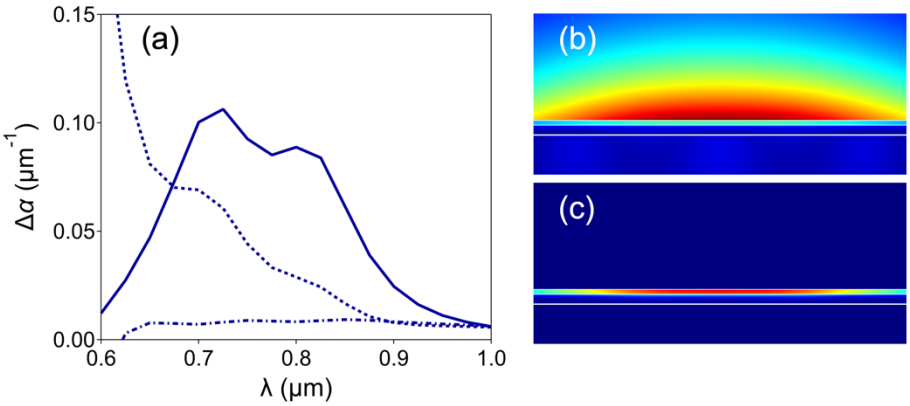

Figure 6: (a) Difference in SPP attenuation $\Delta\alpha$ for dye coated nanostripes compared to bare gold nanostripes. Solid line = resistive heating in the dye-polymer film; dashed line = radiation damping; dot-dashed line = resistive heating in the metal. (b) Plot of the norm of the electric field for dye-PVA coated nanostripes at $\lambda = 0.85$ μm. Only the central portion of the nanostripe is

shown. The different layers from top-to-bottom are air, dye-polymer, Au, Ti (very thin) and silica. (c) Plot of resistive heating in the system at $\lambda = 0.85$ μm.

The simulation results show that the damping of the leaky SPP mode induced by coating with a dye-PVA film has significant contributions from both energy transfer to the dye (resistive heating in the dye-polymer layer) and increased radiation damping. At long wavelengths, near the onset of the dye absorption, energy transfer to the dye is the major effect. The energy transfer process is illustrated in Figure 6(b) and 6(c), where plots of the SPP field and the resistive losses in the system at $\lambda = 0.85$ μm are presented. Figure 6(b) shows that the SPP field extends into the dye-polymer layer, but is strongly attenuated in the metal. Figure 6(c) shows that the field in the dye-polymer layer causes a strong absorption. This corresponds to energy transfer from the SPP mode to the dye. At shorter wavelengths radiation damping becomes increasingly important, and is predicted to be dominant at wavelengths less than 0.7 μm. This means that, in general, effects from both radiation damping and resistive heating needed to be considered in studies of interactions between plasmons and absorbers in thin films. The reason this is important is that to determine the efficiency for energy transfer, the contribution from radiation damping needs to be subtracted from the overall decay rates.

4. Conclusions:

Energy transfer between propagating SPPs of gold nanostripes and dye molecules in a thin PVA film has been examined by scattered light/leakage radiation microscopy. An advantage of these experiments compared to studies of LSPRs is that they provide wavelength resolved lifetime information for a single nanostructure, which is helpful for unravelling the mechanism for the non-radiative processes. The experiments show that the rate of SPP dephasing induced by the dye-PVA layer follows the absorption spectrum of the dye. The measured dephasing rate is very fast, occurring on a time constant of ca. 14 fs at the peak of the dye absorption curve. However, because the decay of the SPP modes is also fast, coherent energy transfer and the formation of hybrid plasmon-exciton states does not occur.[15] We simply see increased SPP decay for this

system. Comparison to finite element simulations, where a Lorentz oscillator model was used for the absorption/dispersion properties of the dye-PVA film,[45] shows that the SPP dephasing has contributions from both energy transfer to the dye and increased radiation damping from the change in the dielectric environment around the nanostripe. Current work is focused on investigating dye or semiconductor systems with larger oscillator strengths. This should increase the rate of energy transfer and allow the formation of hybrid plasmon-exciton states.[16, 23] Understanding the ultrafast decay processes for these states is important for designing and optimizing plasmonic-excitonic systems for applications in sensing, light-harvesting, and photonic devices.

Supporting Information: Diagram of the optical system; momentum matching diagram; Fourier space image and the line profiles; propagation lengths and lifetimes of bare and coated nanostripes; diagram of the model used in the finite element simulations; and details of the Lorentz oscillator model used in the simulations.

Acknowledgements: This work was supported by a grant from the National Science Foundation (CHE-2304905). The nanostructures were fabricated in the Notre Dame Nanofabrication Facility. The authors are grateful for the Smith group at the University of Notre Dame for supplying the near-IR croconaine dye.

References:

1. Maier, S. A., *Plasmonics: Fundamentals and Applications*; Springer Science: New York, 2007.
2. Pelton, M.; Bryant, G., *Introduction to Metal-Nanoparticle Plasmonics*; John Wiley & Sons, Inc: Hoboken, New Jersey, 2013.
3. Gramotnev, D. K.; Bozhevolnyi, S. I., Plasmonics beyond the diffraction limit. *Nature Photonics* **2010**, *4*, 83-91.
4. Barnes, W. L., Surface plasmon-polariton length scales: a route to sub-wavelength optics. *Journal of Optics a-Pure and Applied Optics* **2006**, *8*, S87-S93.
5. Berini, P., Long-range surface plasmon polaritons. *Advances in Optics and Photonics* **2009**, *1*, 484-588.
6. Bozhevolnyi, S. I.; Volkov, V. S.; Devaux, E.; Laluet, J. Y.; Ebbesen, T. W., Channel plasmon subwavelength waveguide components including interferometers and ring resonators. *Nature* **2006**, *440*, 508-511.
7. Boriskina, S. V.; Ghasemi, H.; Chen, G., Plasmonic materials for energy: From physics to applications. *Materials Today* **2013**, *16*, 375-386.
8. Kabashin, A. V.; Evans, P.; Pastkovsky, S.; Hendren, W.; Wurtz, G. A.; Atkinson, R.; Pollard, R.; Podolskiy, V. A.; Zayats, A. V., Plasmonic nanorod metamaterials for biosensing. *Nature Materials* **2009**, *8*, 867-871.
9. Yu, P.; Besteiro, L. V.; Huang, Y. J.; Wu, J.; Fu, L.; Tan, H. H.; Jagadish, C.; Wiederrecht, G. P.; Govorov, A. O.; Wang, Z. M., Broadband Metamaterial Absorbers. *Advanced Optical Materials* **2019**, *7*, 1800995.
10. Vuckovic, J.; Loncar, M.; Scherer, A., Surface plasmon enhanced light-emitting diode. *Ieee Journal of Quantum Electronics* **2000**, *36*, 1131-1144.
11. Lozano, G.; Rodriguez, S. R. K.; Verschuuren, M. A.; Rivas, J. G., Metallic nanostructures for efficient LED lighting. *Light-Science & Applications* **2016**, *5*, e16080.
12. Bellessa, J.; Bonnand, C.; Plenet, J. C.; Mugnier, J., Strong coupling between surface plasmons and excitons in an organic semiconductor. *Physical Review Letters* **2004**, *93*, 036404.
13. Fofang, N. T.; Park, T. H.; Neumann, O.; Mirin, N. A.; Nordlander, P.; Halas, N. J., Plexcitonic Nanoparticles: Plasmon-Exciton Coupling in Nanoshell-J-Aggregate Complexes. *Nano Letters* **2008**, *8*, 3481-3487.
14. Gómez, D. E.; Vernon, K. C.; Mulvaney, P.; Davis, T. J., Surface Plasmon Mediated Strong Exciton-Photon Coupling in Semiconductor Nanocrystals. *Nano Letters* **2010**, *10*, 274-278.
15. Törmä, P.; Barnes, W. L., Strong coupling between surface plasmon polaritons and emitters: a review. *Reports on Progress in Physics* **2015**, *78*, 013901.
16. Baranov, D. G.; Wersall, M.; Cuadra, J.; Antosiewicz, T. J.; Shegai, T., Novel Nanostructures and Materials for Strong Light Matter Interactions. *ACS Photonics* **2018**, *5*, 24-42.
17. Pelton, M.; Storm, S. D.; Leng, H., Strong coupling of emitters to single plasmonic nanoparticles: exciton-induced transparency and Rabi splitting. *Nanoscale* **2019**, *11*, 14540-14552.
18. Collins, S. S. E.; Searles, E. K.; Tauzin, L. J.; Lou, M. H.; Bursi, L.; Liu, Y. W.; Song, J.; Flatebo, C.; Baiyasi, R.; Cai, Y. Y.; et al., Plasmon Energy Transfer in Hybrid Nanoantennas. *ACS Nano* **2021**, *15*, 9522-9530.

19. Jones, A.; Searles, E. K.; Mayer, M.; Hoffmann, M.; Gross, N.; Oh, H.; Fery, A.; Link, S.; Landes, C. F., Active Control of Energy Transfer in Plasmonic Nanorod–Polyaniline Hybrids. *The Journal of Physical Chemistry Letters* **2023**, *14*, 8235-8243.
20. Akselrod, G. M.; Argyropoulos, C.; Hoang, T. B.; Ciracì, C.; Fang, C.; Huang, J. N.; Smith, D. R.; Mikkelsen, M. H., Probing the mechanisms of large Purcell enhancement in plasmonic nanoantennas. *Nature Photonics* **2014**, *8*, 835-840.
21. Kongsuwan, N.; Demetriadou, A.; Chikkaraddy, R.; Benz, F.; Turek, V. A.; Keyser, U. F.; Baumberg, J. J.; Hess, O., Suppressed Quenching and Strong-Coupling of Purcell-Enhanced Single-Molecule Emission in Plasmonic Nanocavities. *ACS Photonics* **2018**, *5*, 186-191.
22. Baumberg, J. J.; Aizpurua, J.; Mikkelsen, M. H.; Smith, D. R., Extreme nanophotonics from ultrathin metallic gaps. *Nature Materials* **2019**, *18*, 668-678.
23. Zengin, G.; Johansson, G.; Johansson, P.; Antosiewicz, T. J.; Käll, M.; Shegai, T., Approaching the strong coupling limit in single plasmonic nanorods interacting with J-aggregates. *Scientific Reports* **2013**, *3*, 3074.
24. Hovel, H.; Fritz, S.; Hilger, A.; Kreibig, U.; Vollmer, M., Width of cluster plasmon resonances - bulk dielectric functions and chemical interface damping. *Phys. Rev. B* **1993**, *48*, 18178-18188.
25. Lee, S. A.; Link, S., Chemical Interface Damping of Surface Plasmon Resonances. *Accounts of Chemical Research* **2021**, *54*, 1950-1960.
26. Foerster, B.; Joplin, A.; Kaefer, K.; Celiksoy, S.; Link, S.; Sönnichsen, C., Chemical interface damping depends on electrons reaching the surface. *ACS Nano* **2017**, *11*, 2886-2893.
27. Martirez, J. M. P.; Bao, J. L.; Carter, E. A., First-Principles Insights into Plasmon-Induced Catalysis. *Annual Review of Physical Chemistry* **2021**, *72*, 99-119.
28. Solis, D.; Chang, W. S.; Khanal, B. P.; Bao, K.; Nordlander, P.; Zubarev, E. R.; Link, S., Bleach-Imaged Plasmon Propagation (BlIPP) in Single Gold Nanowires. *Nano Letters* **2010**, *10*, 3482-3485.
29. Paul, A.; Solis, D.; Bao, K.; Chang, W. S.; Nauert, S.; Vidgerman, L.; Zubarev, E. R.; Nordlander, P.; Link, S., Identification of Higher Order Long-Propagation-Length Surface Plasmon Polariton Modes in Chemically Prepared Gold Nanowires. *ACS Nano* **2012**, *6*, 8105-8113.
30. Wild, B.; Cao, L. N.; Sun, Y. G.; Khanal, B. P.; Zubarev, E. R.; Gray, S. K.; Scherer, N. F.; Pelton, M., Propagation Lengths and Group Velocities of Plasmons in Chemically Synthesized Gold and Silver Nanowires. *ACS Nano* **2012**, *6*, 472-482.
31. Beane, G.; Brown, B. S.; Devkota, T.; Hartland, G. V., Light-like group velocities and long lifetimes for leaky surface plasmon polaritons in noble metal nanostripes. *J. Phys. Chem. C* **2019**, *123*, 15729-15737.
32. Devkota, T.; Brown, B. S.; Beane, G.; Yu, K.; Hartland, G. V., Making waves: Radiation damping in metallic nanostructures. *Journal of Chemical Physics* **2019**, *151*, 080901.
33. Brown, B. S.; Hartland, G. V., Chemical interface damping for propagating surface plasmon polaritons in gold nanostripes. *Journal of Chemical Physics* **2020**, *152*, 024707.
34. Olmon, R. L.; Slovick, B.; Johnson, T. W.; Shelton, D.; Oh, S. H.; Boreman, G. D.; Raschke, M. B., Optical dielectric function of gold. *Physical Review B* **2012**, *86*, 235147.
35. Spence, G. T.; Hartland, G. V.; Smith, B. D., Activated photothermal heating using croconaine dyes. *Chemical Science* **2013**, *4*, 4240-4244.

36. Dickson, R. M.; Lyon, L. A., Unidirectional plasmon propagation in metallic nanowires. *J. Phys. Chem. B* **2000**, *104*, 6095-6098.
37. Sanders, A. W.; Routenberg, D. A.; Wiley, B. J.; Xia, Y. N.; Dufresne, E. R.; Reed, M. A., Observation of plasmon propagation, redirection, and fan-out in silver nanowires. *Nano Letters* **2006**, *6*, 1822-1826.
38. Song, M. X.; Bouhelier, A.; Bramant, P.; Sharma, J.; Dujardin, E.; Zhang, D. G.; Colas-des-Francs, G., Imaging Symmetry-Selected Corner Plasmon Modes in Penta-Twinned Crystalline Ag Nanowires. *ACS Nano* **2011**, *5*, 5874-5880.
39. Wang, Z.; Wei, H.; Pan, D.; Xu, H., Controlling the radiation direction of propagating surface plasmons on silver nanowires. *Laser & Photonics Reviews* **2014**, *8*, 596-601.
40. Yang, H.; Qiu, M.; Li, Q., Identification and control of multiple leaky plasmon modes in silver nanowires. *Laser & Photonics Reviews* **2016**, *10*, 278-286.
41. Wei, H.; Pan, D.; Zhang, S.; Li, Z.; Li, Q.; Liu, N.; Wang, W.; Xu, H., Plasmon Waveguiding in Nanowires. *Chemical Reviews* **2018**, *118*, 2882-2926.
42. Zhang, S.; Xu, H., Optimizing Substrate-Mediated Plasmon Coupling toward High-Performance Plasmonic Nanowire Waveguides. *ACS Nano* **2012**, *6*, 8128-8135.
43. Johnson, P. B.; Christy, R. W., Optical constants of noble metals. *Physical Review B* **1972**, *6*, 4370-4379.
44. Berini, P., Figures of merit for surface plasmon waveguides. *Optics Exp.* **2006**, *14*, 13030-13042.
45. Gentile, M. J.; Núñez-Sánchez, S.; Barnes, W. L., Optical Field-Enhancement and Subwavelength Field-Confinement Using Excitonic Nanostructures. *Nano Letters* **2014**, *14*, 2339-2344.

TOC Graphic: